Photosynthesis Research (2024) 162:13–27
https://doi.org/10.1007/s11120-024-01112-7

RESEARCH

Mg^{2+} limitation leads to a decrease in chlorophyll, resulting in an unbalanced photosynthetic apparatus in the cyanobacterium *Synechocytis* sp. PCC6803

Anne-Christin Pohland[1,3] · Gábor Bernát[3] · Stefan Geimer[4] · Dirk Schneider[1,2]

Received: 26 April 2024 / Accepted: 14 July 2024 / Published online: 22 July 2024
© The Author(s) 2024

Abstract
Mg^{2+}, the most abundant divalent cation in living cells, plays a pivotal role in numerous enzymatic reactions and is of particular importance for organisms performing oxygenic photosynthesis. Its significance extends beyond serving as the central ion of the chlorophyll molecule, as it also acts as a counterion during the light reaction to balance the proton gradient across the thylakoid membranes. In this study, we investigated the effects of Mg^{2+} limitation on the physiology of the well-known model microorganism *Synechocystis* sp. PCC6803. Our findings reveal that Mg^{2+} deficiency triggers both morphological and functional changes. As seen in other oxygenic photosynthetic organisms, Mg^{2+} deficiency led to a decrease in cellular chlorophyll concentration. Moreover, the PSI-to-PSII ratio decreased, impacting the photosynthetic efficiency of the cell. In line with this, Mg^{2+} deficiency led to a change in the proton gradient built up across the thylakoid membrane upon illumination.

Keywords *Synechocystis* · Mg^{2+} limitation · PQ pool · Electron transport · ΔpH · Acridine orange

Introduction

Mg^{2+} is the most abundant divalent cation in living cells (Wacker 1969). In mammalian cells, the total Mg^{2+} concentration ranges between 17 and 20 mM (Romani and Scarpa 2000), whereas it is reportedly higher in bacterial cells where it ranges between 15 and 200 mM (Lusk et al. 1968; Silver 1969; Kung et al. 1976; Moncany and Kellenberger 1981). Within cells, most of the Mg^{2+} is bound to macromolecules (Flatman 1984), and only ~4 mM Mg^{2+} is "free" (Lusk et al. 1968). It is estimated that around 50% of the cellular Mg^{2+} is bound to ATP (Maguire and Cowan 2002), forming an ATP-Mg^{2+} complex, the biologically active ATP form. This makes Mg^{2+} extremely important for cellular bioenergetics. In plants, Mg^{2+} is an essential macronutrient (Merhaut 2007) and of particular importance for photosynthesis, as Mg^{2+} is part of chlorophyll (Chl) (Willstätter 1906), an essential pigment involved in light harvesting and photosynthetic light reactions. Consequently, reducing the amount of available Mg^{2+} results in a reduced amount of Chl in both algae and plants (Finkle and Appleman 1953; Kobayashi and Tanoi 2015; Peng et al. 2019; Giraldo et al. 2021). In line with a reduced Chl content, a decrease in the maximum quantum yield of photosystem II (PSII) has been observed in some plants (Hermans et al. 2004; Yang et al. 2012; Tang et al. 2012; Tränkner and Jamali Jaghdani 2019), as well as reduced photosynthetic CO_2 fixation rates (Cakmak and Kirkby 2008). Additionally, the overall PSI activity was decreased due to a significantly reduced PSI abundance (Hermans et al. 2004; Farhat et al. 2015).

Plastids have evolved from a cyanobacterial ancestor (Schimper 1883; Mereschkowsky 1905; Sagan 1967; Gray 1989), and consequentially, the structures of modern-days

✉ Dirk Schneider
Dirk.Schneider@uni-mainz.de

1 Department of Chemistry, Biochemistry, Johannes Gutenberg University Mainz, Hanns-Dieter-Hüsch-Weg 17, Mainz 55128, Germany

2 Institute of Molecular Physiology, Johannes Gutenberg University Mainz, Mainz, Germany

3 HUN-REN Balaton Limnological Research Institute, Tihany, Hungary

4 Cell Biology and Electron Microscopy, University of Bayreuth, Bayreuth, Germany

cyanobacteria and chloroplasts are highly similar in many aspects. Cyanobacteria have a unique and highly differentiated internal membrane system compared to other bacteria. The cyanobacterial cell envelope has a typical Gram-negative membrane organization, consisting of an inner cytoplasmic membrane (CM), which is equivalent to the chloroplast inner envelope membrane, a peptidoglycan layer, and an outer membrane (OM). Furthermore, most cyanobacteria contain a separated internal membrane system that is also found in chloroplasts, the thylakoid membranes (TMs), where the pigment-protein complexes of the photosynthetic electron transport network are located (Liu 2016). As in plants, Mg^{2+} is an essential nutrient also in cyanobacteria (Pohland and Schneider 2019), and the lower limit for growth of the cyanobacterium *Synechococcus elongatus* (*S. elongatus*, formerly: *Anacystis nidulans*) is around 5 µM Mg^{2+} (Utkilen 1982). Mg^{2+} deficiency resulted in a lowered amount of total proteins in the cyanobacteria *Cyanothece* strain 16Som2 and *Cyanospira capsulata*, accompanied by a significant enhancement of the exopolysaccharide (EPS) production in the latter (De Philippis et al. 1991). Furthermore, as observed in plants, the PSII activity was also reduced in the cyanobacterium *Arthrospira platensis* Gomont 1892 when cells were grown in medium with a low Mg^{2+} content (Urek and Kerimoglu 2019).

TMs are composed of four major lipids, two of which have a negatively charged head group (Sakurai et al. 2006). This results in a negatively charged membrane surface, which is mainly screened by loosely bound Mg^{2+} ions (Pottosin and Dobrovinskaya 2015; Kaňa and Govindjee 2016). In plants, Mg^{2+} is crucial for grana stacking, and the observed altered photosynthesis at low Mg^{2+} concentrations might be caused by the disruption of grana stacks (Hall et al. 1972; Jennings et al. 1978).

During the TM-associated photosynthetic light reaction, light energy is captured and used to drive electron transport from water to nicotinamide adenine dinucleotide phosphate through photosynthetic pigment-protein complexes, i.e., PSII, the cytochrome b_6f complex, and PSI, as well as mobile electron carriers. The photosynthetic electron transport is tightly coupled to H^+ translocation from the chloroplast stroma or the cyanobacterial cytoplasm, respectively, into the thylakoid lumen, resulting in acidification of the lumen and generation of a proton gradient (ΔpH) across the membrane, as initially proposed by Peter Mitchell (Mitchell 1961). A Mg^{2+} efflux from the chloroplast TM lumen electrically compensates for the light-generated ΔpH formation in plant chloroplasts (Dilley and Vernon 1965; Hind et al. 1974; Barber et al. 1974; Chow et al. 1976; Portis and Heldt 1976). Besides counterbalancing the ΔpH across TMs, Mg^{2+} can also regulate the activity of several chloroplast enzymes involved in CO_2 fixation, such as Ribulose-1,5-bisphosphate carboxylase/oxygenase, fructose 1,6-bisphosphatase, and sedoheptulose 1,7-bisphosphatase (Portis et al. 1977; Portis 1992). Although not yet experimentally demonstrated, the intracellular Mg^{2+} concentration may also vary in cyanobacteria depending on the light conditions, as observed in chloroplasts. Moreover, unlike in chloroplasts, there is active respiratory electron flow in cyanobacteria, whose components are also localized in the TMs (for a review, see (Mullineaux 2014). This results in a ΔpH of about 2 units across the TM already in the dark (Peschek et al. 1985; Belkin et al. 1987), albeit the thylakoid lumen is further acidified upon illumination, with a decrease of at least 0.5 pH units (Belkin et al. 1987; Teuber et al. 2001).

In contrast to plants, the research on cyanobacteria has thus far primarily focused on the impact of limited Mg^{2+} availability on growth and biomass production (Utkilen 1982; De Philippis et al. 1991; Philippis et al. 1993), while its effects on photosynthetic light reactions have not yet been explored in detail.

Here, we have analyzed the impact of Mg^{2+} limitation on growth and photosynthetic performance of the cyanobacterium *Synechocystis* sp. PCC6803 (from hereon: *Synechocystis*). When *Synechocystis* wild type cells were grown under Mg^{2+} limitation, both cell growth and photosynthetic activity were affected, in line with a reduced Chl *a* content. Furthermore, measuring light-induced pH changes using the fluorescent dye acridine orange (AO) revealed a distinct change in the pH gradient across the TM under Mg^{2+} limiting conditions. This highlights the involvement of Mg^{2+} in counterbalancing the ΔpH established across the TMs.

Materials and methods

Growth conditions

For the growth analyses, 25 mL cultures of glucose-tolerant *Synechocystis* wild type cells were grown in 50 mL Erlenmeyer flasks in a temperature-controlled incubation shaker (Multitron HT, Infors (Bottmingen, Switzerland) at 130 rpm and 30 °C under constant illumination of 120 µmol photons m^{-2} s^{-1}. *Synechocystis* cells were grown without glucose either in a modified BG11 medium (modified from (Rippka et al. 1979) see Supplementary Table 1) including 300 µM Mg^{2+} and 5 mM HEPES/KOH pH 8.0 (from now on BG11) or, for growth under Mg^{2+} limiting conditions, in BG11 with decreased Mg^{2+} concentration where $MgSO_4$ was replaced by Na_2SO_4 and a defined amount of Mg^{2+} ($MgCl_2$) was added afterwards. Here, the final Mg^{2+} concentration ranged from 10 to 70 µM. Growth of *Synechocystis* was monitored by measuring the optical density at

750 nm (OD_{750}). For each growth condition, three biological replicates were monitored.

For all other analyses, cyanobacterial cells were grown photoautotrophically at constant cell density ($OD_{720} = 1.0$) in a multi-cultivator (Multi-Cultivator MC 1000-OD, Photon Systems Instruments (PSI), Drásov, Czechia) equipped with a Turbidostat TS-1000 (PSI, Drásov, Czechia), bubbled with 5% (v/v) CO_2 in air at 30 °C (controlled by a Cooling Unit AC-710 (PSI, Drásov, Czechia)). The intensity of the (white) growth light was set to 30 µmol photons m^{-2} s^{-1}. Cells were grown either in BG11 with 300 µM Mg^{2+} or, under Mg^{2+} limitation, in BG11 media supplemented with 50 µM Mg^{2+}. Prior to the measurements, cells were centrifuged at 1800 *g* at room temperature (RT) for 10 min, and the cell pellet was solubilized in fresh medium with the OD_{750} adjusted to 2.0.

Electron microscopy

Electron microscopic (EM) images were acquired by using whole cells grown under high and low Mg^{2+} conditions. 20 mL of a cell suspension was spun down at 1800 *g* for 10 min at RT. The supernatant was removed, and the cells were washed with 20 mM HEPES/KOH pH 7.0. After another centrifugation, the cells were resuspended in the same medium with a final OD_{750} of 5.0. The suspension was then mixed 1:1 with 10% glutaraldehyde. The fixed samples were sedimented at 3300 *g* for 10 min, washed with bi-distilled (bidest.) water at RT for 10 min, and then spun down again. The cells were post-fixed with 2% OsO_4 (w/v in bidest. water) for 120 min at 4 °C. Thereafter, the samples were centrifuged for 10 min at 6600 g and washed with bidest. water three times. Cells grown at low Mg^{2+} conditions were infiltrated with 20% bovine serum albumin for 120 min at 4 °C, centrifuged for 10 min, and fixed in 5% glutaraldehyde in 0.05 M phosphate buffer pH 7.5 to obtain a dense pellet. All samples were then taken up in 2% agar, cut into small blocks, and washed in bidest. water for 5 min. The samples were dehydrated in ethanol of increasing concentrations. After dehydration, the solvent was replaced with a gradually increasing concentration of epon resin. After that, the samples were left in an embedding capsule for 2–3 days at 60 °C. Ultrathin sections were cut with an Ultracut EM UCT ultramicrotome (Leica Microsystems, Wetzlar, Germany) using a diamond knife (Type Ultra 45°, Diatome, Biel, Switzerland). Sections were collected on pioloform-coated copper slotted grids (Plano, Wetzlar, Germany) and stained with uranyl acetate and lead citrate (Reynolds 1963). Cells were imaged using a JEM-1400Plus transmission electron microscope (JEOL (Tokyo, Japan) operated at 80 kV and equipped with a JEOL Ruby CCD camera (3,296 × 2,472 pixels).

Cell counting

For cell counting, cultures were diluted 20-fold in the appropriate growth medium, and 10 µL were loaded into a counting chamber (Thoma scale). After cells had settled, cells were counted regularly to determine the mean cell density of at least three biological replicates.

Determination of pigment composition

To determine the Chl *a* and carotenoid (Car) contents, an equivalent of 500 µL culture with an OD_{750} of 2.0 was harvested *via* centrifugation for 10 min at 16,000 *g* at RT. The supernatant was discarded, and 1.0 mL of 100% methanol was added to the pellet. Then, the sample was rigorously vortexed and incubated on a platform shaker (Duomax 1030 Heidolph, Schwabach, Germany) at RT for 15 min. After an additional centrifugation step for 10 min at 16,000 *g* and 4 °C, the absorption (A) of the supernatant at 665.2 nm and 652 nm (for Chl *a*), and 470 nm and 720 nm (for Car) was measured in a standard 10 mm polystyrene cuvette using a Perkin Elmer, Lambda 435 spectrophotometer (PerkinElmer, Rodgau, Germany). The Chl *a* concentration was determined according to (Porra et al. 1989):

$$Chl\ a\ \left[\frac{\mu\, g}{mL}\right] = 16.26 * A_{665.2} - 8.54 * A_{652} \tag{1}$$

The Car concentration was determined according to (Zavrel et al. 2015):

$$Car\left[\frac{\mu\, g}{mL}\right] = \left[\frac{1{,}000\,(A_{470} - A_{720}) - 2.86\,\left(Chl\ a\ \left[\frac{\mu g}{mL}\right]\right)}{221}\right] \tag{2}$$

Whole-cell absorbance spectra

Spectra of whole cells were recorded using a Perkin-Elmer Lambda 35 (PerkinElmer, Rodgau, Germany) spectrophotometer equipped with an integrating sphere. Spectra were recorded in the 300–800 nm spectral region and the absorbance value at 800 nm was subtracted. After normalization to the Chl *a* absorbance at 678 nm the molar phycocyanin (PC)-to-Chl *a* ratio was calculated according to (Rakhimberdieva et al. 2001).

$$PC\ :\ Chl\ a = \frac{4.9\,A_{625} - 2.1\,A_{652} - 0.8\,A_{678}}{0.1\,A_{625} - 0.7\,A_{652} + 15.8\,A_{678}} \tag{3}$$

Low temperature (77 K) fluorescence emission spectroscopy

Low-temperature fluorescence emission spectra were recorded using an Aminco Bowman Series 2 fluorimeter equipped with a 77 K accessory. 1 mL of a cell suspension with an OD_{750} of 2.0 was filled into a glass tube and shock frozen in liquid nitrogen. Chl *a* and phycobilisomes (PBS) were excited at 435 nm and 580 nm, respectively. Spectra were recorded in the 630–760 nm spectral range. The spectra were baseline corrected and normalized to the 695 nm and 665 nm emission upon Chl *a* and PBS excitation, respectively. For further evaluation, the peak areas of the PSII and PSI emissions, centered at 695 nm and 725 nm, respectively, upon Chl *a* excitation were integrated using the Fityk curve fitting software (Wojdyr 2010). The ratio of these areas can be considered equivalent to the PSII : PSI molar ratio (Murakami 1997). The cellular PSI and PSII contents (in mol $cell^{-1}$), in turn, were estimated as described in (Luimstra et al. 2019), which approach exploits this ratio, as well as the cellular Chl *a* content (in mol $cell^{-1}$) and number of Chl *a* molecules per PSI (100) and PSII (35) reaction center (Jordan et al. 2001; Umena et al. 2011; Malavath et al. 2018; Gisriel et al. 2022).

$$PSI_{Cell} = \frac{[Chl\ a]}{100 + 35\ /\ (PSI\ :\ PSII)} \quad (4)$$

$$PSII_{Cell} = \frac{[Chl\ a]}{100\ (PSI\ :\ PSII) + 35} \quad (5)$$

Oxygen (O_2) yield measurements

Photosynthetic O_2 evolution was determined in a custom-made, thermo-regulated chamber using a fiber-optic O_2 meter (PreSens, Regensburg, Germany) at 30 °C. The optode was calibrated with air-saturated (100% O_2) and O_2-free water (0% O_2, obtained upon the addition of sodium thiosulfate). Samples were dark incubated for 15 min prior to the measurements. 10 mM sodium bicarbonate ($NaHCO_3$) was added as an electron acceptor. The recordings started with measuring the O_2 consumption in the dark, followed by monitoring O_2 production upon strong light exposure (3000 K; KL 2500 LCD, Schott, Mainz, Germany). The net O_2 evolution was determined by subtracting the slope of the signal during the dark from the slope of the subsequent O_2 evolution.

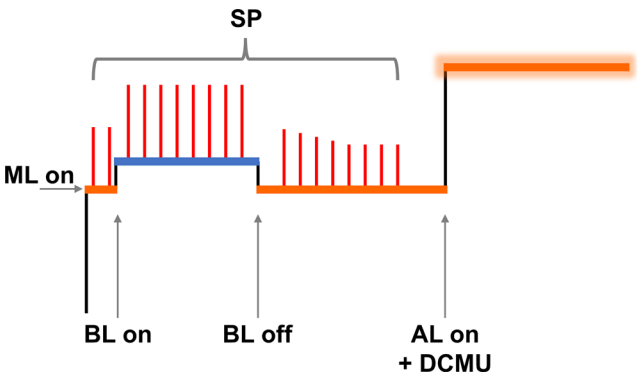

Fig. 1 Schematic view of a fluorescence induction curve with the applied lights and saturating pulses on top. ML, Measuring light (I = 2 µmol photons m^{-2} s^{-1}); BL, weak blue light (I = 29 µmol photons m^{-2} s^{-1}); SP, saturating pulse (I = 10,000 µmol photons m^{-2} s^{-1}); AL, strong red actinic light (I = 187 µmol photons m^{-2} s^{-1}); DCMU, 3-(3,4-dichlorophenyl)-1,1-dimethylurea

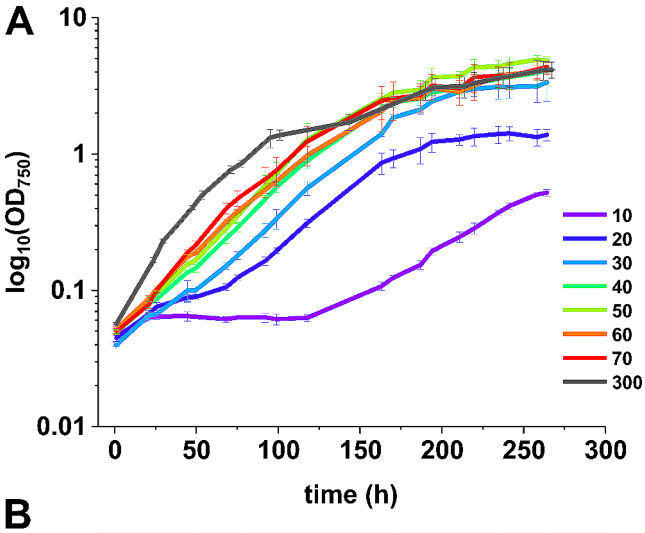

B

Mg^{2+} (µM)	10	20	30	40	50	60	70	300
T_d (h)	44.2	35.5	31.0	29.5	24.7	28.0	25.3	25.9
± SD	1.4	2.1	0.8	0.9	1.6	1.5	2.4	1.3

Fig. 2 Growth of *Synechocystis* at different Mg^{2+} concentrations. (**A**) Growth curves of *Synechocystis* at different Mg^{2+} concentrations with the Mg^{2+} concentration in the growth medium (in µM) shown next to the color bars. (**B**) Doubling times (T_d) at different Mg^{2+} concentrations. Error bars represent the standard deviation (SD) of the mean ($N = 3$)

Pulse amplitude modulation (PAM) fluorometry

PSI and PSII associated quantum yields were determined using a Dual-PAM-100 measuring system equipped with Dual-E and DUAL-DR modules (Walz GmbH, Effeltrich, Germany). The maximum quantum yield of PSII (F_v/F_m) (Kitajima and Butler 1975) was determined by recording fluorescence induction curves at RT (Table 1; Fig. 1) after 5 min of dark acclimation. The initial fluorescence, F_o, and

the maximal fluorescence under actinic light upon addition of 3-(3,4-dichlorophenyl)-1,1-dimethylurea (DCMU) (Campbell et al. 1998), F_m, were used for the determination of F_v/F_m.

$$Fv/Fm = (Fm - Fo)/Fm \tag{6}$$

Furthermore, weak blue light was used to induce state 1 transition (Schreiber et al. 1995). During each phase 600 ms saturating light pulses were applied on top to follow the corresponding maximal signal intensity (I = 10,000 µmol photons m^{-2} s^{-1}).

The effective quantum yield of PSI (Y(I), the PSI quantum yield with donor and acceptor side limitations (Y(ND) and Y(NA), respectively), and the effective PSII quantum yield (Y(II) were determined *via* recording rapid light curves by the Dual-PAM-100 system. Here, the actinic light intensities increased stepwise from 0 to 827 µmol photons m^{-2} s^{-1}. Steady state (F_s) and maximal (F_m') fluorescence levels were determined after 30 s illumination period at each light intensity where 300 ms saturating pulses with an intensity of 10,000 µmol photons m^{-2} s^{-1} were applied. The corresponding PSI parameters, i.e. the maximum amplitude of the P_{700} signal after far red illumination (P_m), the steady state (P) and maximum (P_m') P_{700} signal under illumination were determined concomitantly. Parameters were calculated according to (Genty et al. 1989; Klughammer and Schreiber 2008).

$$Y(I) = (Pm' - P)/Pm \tag{7}$$

$$Y(ND) = (P)/Pm' \tag{8}$$

$$Y(NA) = (Pm - Pm')/Pm \tag{9}$$

$$Y(II) = (Fm' - Fs)/Fm' \tag{10}$$

P_{700} re-reduction kinetics

P_{700} re-reduction kinetics were measured using a Dual-PAM-100 measuring system (Klughammer and Schreiber 1994). Complete P_{700} oxidation was achieved by a 100-ms saturating pulse (I = 10,000 µmol photons m^{-2} s^{-1}). P_{700}^+ decay kinetics were fitted with single exponential functions to determine the corresponding rate constant (*k*).

Acridine orange (AO) fluorescence measurements

The magnitude and kinetics of pH changes within *Synechocystis* cells upon illumination were monitored using the fluorescent dye AO (Teuber et al. 2001) with a Dual-PAM-100 measuring system equipped with an Acridine Orange/Yellow fluorescence emitter-detector module. For each measurement, 1.5 mL cell suspension was mixed with 100 µL of Tricine buffer (1 M, pH 8.0) and 1 µL of an AO solution (10 mM), in a 10 mm quartz cuvette. Each measurement is preceded by a 15-minute dark incubation. After starting the measurements, cells were kept for another three minutes in the dark, then red AL with an intensity of 216 µmol photons m^{-2} s^{-1} was provided for five minutes. Eventually, AO fluorescence was recorded for another two minutes in the dark. Spectra were baseline corrected and normalized to the fluorescence intensity monitored during the first three minutes in the dark.

Results

Mg^{2+} is essential for the cell growth of Synechocystis

To first elucidate the importance of Mg^{2+} for cell viability, *Synechocystis* cells were grown in standard growth medium as well as in media with reduced Mg^{2+} contents, and cell growth was monitored.

BG11, the standard growth medium of *Synechocystis*, contains a Mg^{2+} concentration of about 300 µM (Rippka et al. 1979); we refer to this as "high Mg^{2+}" (HM) from hereon. As shown in Fig. 2A, *Synechocystis* has the highest growth rates at this condition. With decreasing Mg^{2+} concentrations *Synechocystis* is still able to grow, even at a Mg^{2+} concentration of as low as 10 µM, albeit at low Mg^{2+} concentrations the maximal culture densities, expressed as OD_{750}, decreased significantly and cells reached a stationary phase later compared to standard conditions. When grown in the presence of 10 µM Mg^{2+} in the growth medium the doubling time (T_d) was about 1.7 times longer (44.2 ± 1.4 h) compared to the control (HM, T_d = 25.9 ± 1.3 h) (Fig. 2B). Furthermore, a prolonged initial lag phase can be observed at Mg^{2+} concentrations below 40 µM. Above this concentration, the growth characteristics were similar to HM conditions, and thus, we decided to use 50 µM Mg^{2+} (low Mg^{2+}, LM) in the culture medium for all subsequent measurements to ensure the survival of *Synechocystis* cells under Mg^{2+} limiting growth conditions. Noteworthy, while *Synechocystis* cultures grew well under LM conditions, a massive EPS-layer, composed of secreted (exo) polysaccharides (EPS), surrounding the individual cells accumulated when cells were grown under LM conditions (Fig. 3).

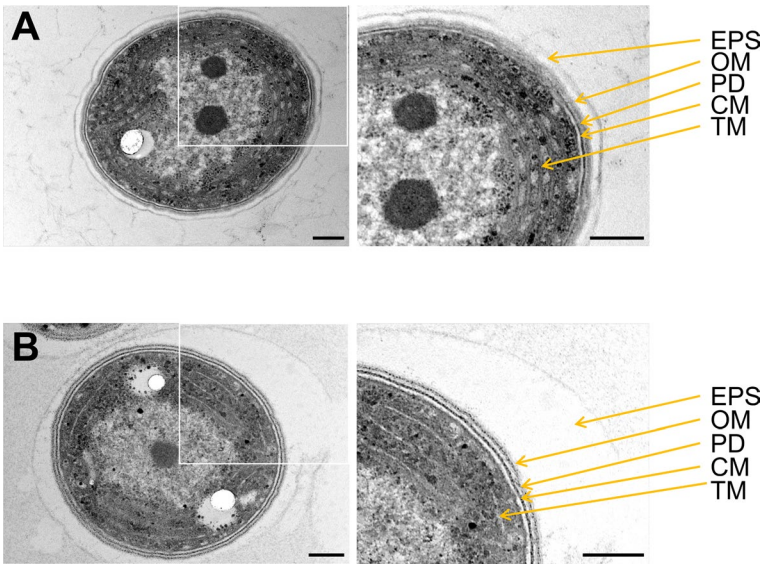

Fig. 3 EM images of *Synechocystis* cells grown in HM or LM medium. Compared to standard growth conditions (**A**), whole cell images show an extensive exopolysaccharide layer (EPS) when cells were grown under Mg^{2+}-limiting conditions (**B**). Images on the right show magnification of the boxed areas of the corresponding images on the left. EPS, exopolysaccharide; OM, outer membrane; PD, peptidoglycan layer; CM, cytoplasmic membrane; TM, thylakoid membrane. Scale bars = 200 nm

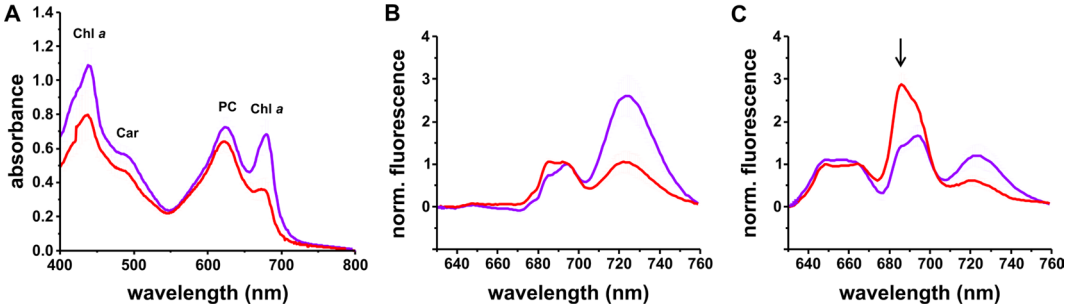

Fig. 4 Absorbance and 77 K fluorescence spectra of intact *Synechocystis* cells grown under HM or LM conditions. (**A**) In the absorbance spectra, the reduction in Chl *a* concentration under LM (red) compared to HL (blue) conditions is visible as decreased peak intensities at 437 nm and 678 nm. An increase in the PC-to-Chl *a* ratio can also be observed. The absorbance maxima of the respective pigments are indicated for comparison. Chl *a*, chlorophyll *a*; Car carotenoids; PC, phycocyanin. Error bars represent means ± SD ($N = 6$ (HM); $N = 3$ (LM)). (**B**) 77 K fluorescence emission spectra were recorded upon Chl excitation at 435 nm and normalized to 695 nm. Mg^{2+} limitation (red) resulted in a decreased PSI-to-PSII ratio. (**C**) 77 K spectra after PBS excitation at 580 nm and normalization to 665 nm revealed altered PC-to-PSI and PC-to-PSII ratios under Mg^{2+} limitation (red). The arrow marks the peak that presumably shows uncoupled PBS (as further discussed in the text). Error bars represent means ± SD ($N = 5$ (HM); $N = 3$ (LM))

Content and composition of pigment-containing protein complexes involved in photosynthesis

When *Synechocystis* cells were grown in LM medium, the absorbance spectra of whole cells differed significantly from spectra of HM-grown cells: the characteristic Chl *a* absorbance maxima at 437 nm and 678 nm were severely reduced, indicating a highly reduced Chl *a* content, which suggests a lower cellular abundance of Chl *a*-containing protein complexes, i.e. PSs (Fig. 4A). The PC-to-Chl *a* ratio increased from 0.19 ± 0.03 under HM conditions to 0.38 ± 0.05 under LM conditions calculated from normalized spectra, as described in Material and Methods.

The decreased Chl *a* content observed in the absorbance spectra of LM cultures was confirmed by spectroscopic analyses of methanolic cell extracts (Supplementary Fig. 1). The cellular Car content, which is visible as a shoulder at 480 nm in the whole cell absorbance spectra (Fig. 4A), was also reduced in the LM cultures, albeit to much lower extents (Supplementary Fig. 1B). Thus, the calculated Chl *a*-to-Car ratio was lower in LM grown cells compared to HM grown (Supplementary Fig. 1C).

Next, we analyzed the relative abundance of the two PSs, as well as energy transfer from (PBS) to PSI and PSII *via* low temperature (77 K) fluorescence spectroscopy. Cyanobacteria regulate the energy distribution between the two PSs by adjusting their soluble antenna systems, the PBS which consist of six rods of phycocyanin (PC) and one core of allophycocyanin (APC) (Kirilovsky et al. 2014; Calzadilla and Kirilovsky 2020). PBSs are primarily associated with PSII when the PQ pool is oxidized (state I) and with PSI when the PQ pool is reduced (state II) (Mullineaux and Allen 1990).

Upon excitation of Chl *a* at 435 nm, the HM cultures exhibit fluorescence emission spectra typical for *Synechocystis* (Fig. 4B) with main emission peaks at around 685 nm, 695 nm, and 725 nm, which originate from the PSII core antennas CP43 and CP47 and (to some extent) the PBS terminal emitter (at 685 nm), CP47 of PSII (695 nm), and PSI (725 nm), respectively (Rijgersberg and Amesz 1980; Shen et al. 1993; Andrizhiyevskaya et al. 2005). Under LM conditions, the decrease in the relative fluorescence emission at 725 nm indicates a reduced relative amount of PSI. This is in good agreement with the observation that about 90% of the total Chl *a* in *Synechocystis* is bound by PSI (Jordan et al. 2001; Umena et al. 2011; Zakar et al. 2018; Malavath et al. 2018). To quantify the relative changes in the cellular abundance of the PSs, we next calculated the photosystem per cell content as described in Material and Methods. According to the results, the number of PSII/cell hardly changed under LM conditions compared to HM conditions (0.030 ± 0.002 10^{-18} mol/cell ($N=4$) vs. 0.031 ± 0.002 10^{-18} mol/cell ($N=3$), respectively). In contrast, the number of PSI decreased significantly from $(0.27 \pm 0.03) \times 10^{-18}$ mol/cell (HM, $N=4$) to $(0.10 \pm 0.02) \times 10^{-18}$ mol/cell (LM, $N=3$). In line with the lowered cellular PSI content, a decreased energy transfer from PBS to PSI was observed upon PBS excitation at 580 nm (Fig. 4C). Meanwhile, the fluorescence emission at 685 nm and 695 nm increased, indicating an increased PBS-to-PSII energy transfer. Nevertheless, as the PBS terminal emitter may also contribute to the 685 nm fluorescence emission signal, this increased fluorescence emission intensity rather suggests an increased abundance of uncoupled PBSs, as observed previously (Mullineaux 1994; Barthel et al. 2013; Kłodawska et al. 2020), in line with an increased relative PC content (Fig. 4A).

The activity of photosystem I and II

While an altered PSI-to-PSII ratio was indicated, it remained unclear whether Mg^{2+} limitation has an impact of the activity of the respective PS.

The activity of PSII was analyzed by recording fluorescence induction curves. While the method, in principle, probes the redox state of Q_A, the primary electron acceptor of PSII, it also probes the redox state of the PQ pool as well as the status of the entire electron transport chain and the antenna systems (Schreiber 2004).

At first, the maximum PSII quantum efficiency F_v/F_m was determined, an often used proxy to characterize the PSII performance in plants (Maxwell and Johnson 2000) as well as in cyanobacteria (Campbell et al. 1998). As shown in Fig. 5, both the initial ("minimal") fluorescence yield F_o as well as the maximum fluorescence yield upon illumination (F_m') were higher in LM grown *Synechocystis* cells compared to cells grown under HM conditions. Yet, as the applied measuring light ($\lambda_{ex} = 620$ nm) excites not only Chl *a* molecules but also PBSs, PBS fluorescence emission may also significantly contribute to the higher F_o value (Campbell et al. 1996). The observed increase in the PC-to-Chl *a* ratio seen in the absorbance spectra (Fig. 4A) and the higher amount of uncoupled PBS observed in the 77 K fluorescence emission measurements (Fig. 4C) are in line with this assumption. In the case of the HM cultures, the F_m' values determined under blue light illumination were very similar to the values determined under red light in the presence of DCMU, while in the LM cultures, these were substantially lower. This suggests a less effective state I transition in the LM cultures, most likely due to the lower abundance of PSI, which is crucial for the oxidation of one key element of state transitions, the PQ pool.

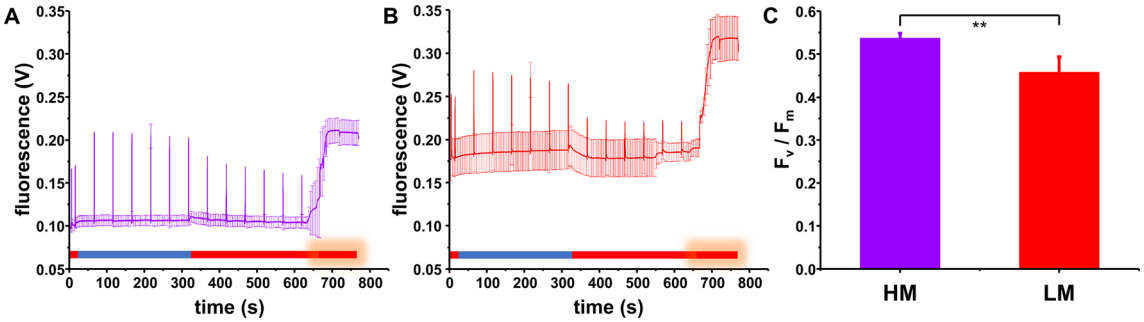

Fig. 5 Fluorescence induction curves and the maximal PSII quantum yield of *Synechocystis* cells grown under HM and LM conditions. (**A**, **B**) Averaged traces of fluorescence induction curves measured with HM (**A**) or LM (**B**) cultures. The color bar below the traces indicates the light quality as described in Material and Methods. For clarity, only every 150th data point is displayed. After dark incubation cells were illuminated with low intensity measuring light, and a saturating light pulse was given. Then weak blue light was turned on to induce state I transitions. Saturating light pulses were given repeatedly to monitor changes in maximum fluorescence. Next the blue light was turned off, and saturating light pulses were kept being given to follow the transition back to state II. After the addition of DCMU, continuous actinic light was turned on, F_m was determined and the maximal quantum yield was estimated (**C**). The higher PC-to-Chl *a* ratio and the abundance of uncoupled PBS likely resulted in an overall higher signal under LM conditions. Error bars represent means ± SD ($N=4$ (HM); $N=6$ (LM)). Significant differences (according to Student's t-test) are indicated as: ** $p < 0.01$

In line with this, in LM grown cells some fluorescence quenching was observed upon blue light illumination (Fig. 5B). The F_v/F_m values (maximal PSII quantum yields) calculated based on F_o and the maximum fluorescence yields obtained in the presence of DCMU (F_m) were slightly smaller in the LM compared to the HM cultures (Fig. 5C). However, this is most likely due to the enhanced F_o level. To further analyze the PSII activity, we next applyed rapid light curves to probe energy conversion efficiency at different light intensities. The effective quantum yield of PSII (Y(II)), which indicates the quantity of absorbed light that is "used" by PSII, was decreased when cells were grown under LM conditions (Fig. 6A).

Next, we measured O_2 evolution rates using intact *Synechocystis* cells grown either under LM or HM conditions (Fig. 6B). As the PSII contents per cell were rather similar, yet the Chl *a* concentration differed between the HM and LM cultures, we decided to express the O_2 yields as µmol O_2 L^{-1} min^{-1} at an $OD_{750}=2.0$ (see Supplementary Fig. 4 for oxygen evolution rate per cell). Compared to HM conditions, the net oxygen evolution rate was significantly reduced under LM conditions, in line with the Y(II) measurements. Yet, Mg^{2+}-limitation influenced respiration much more than O_2 production, thus, the observed lower apparent O_2 production rates in cells grown under LM conditions were mainly due to reduced O_2 consumption, in excellent agreemen with the observation that the PSII content per cell is largely unchanged.

While the activity of PSII was only slightly affected, we subsequentely focused on the activity of PSI. Due to a significant decrease in the amount of PSI under LM conditions, we anticipated a changed activity. To study the electron transport to and from PSI at different light intensities, we applied rapid light curves. With increasing light intensities the effective quantum yield of PSI (Y(I)) decreases less prominently in the LM grown cultures compared to the HM grown cells, due to a lower donor side limitation, Y(ND), while limitations at the acceptor side Y(NA) were negligible under both conditions (Fig. 7A). This implies that in cells grown under LM conditions, electron shortage is less pronounced and more electrons arrive at PSI to reduce P_{700}^+ to P_{700}. The lowered Y(ND) is in agreement with a reduced PSI content. The reduced number of oxidizable P_{700} centers in LM grown cells is also evident by two features visible in P_{700}/P_{700}^+ oxidation/re-reduction kinetic measurements (Fig. 7B, C): (i) by the decreased P_m intensities /Fig. 7B) and (ii) by the faster P_{700} re-reduction kinetics (Fig. 7C) due to the decreased PSI-to-PSII ratio (Fig. 4B).

Mg^{2+} limitation affects the ΔpH established across thylakoid membranes

Mg^{2+} depletion affects the PS stoichiometry, and thus electron transport properties, plus Mg^{2+} is essential to counterbalance the ΔpH built-up across the TM driven by photosynthetic electron transport (Dilley and Vernon 1965; Hind et al. 1974; Barber et al. 1974; Chow et al. 1976; Portis and Heldt 1976). Consequentely, we next analyzed whether Mg^{2+} limitation affected formation of the ΔpH using the fluorescent dye acridine orange (AO) (Fig. 8), as described in Teuber et al. (Teuber et al. 2001). Upon turning on actinic light, a rapid drop in the AO fluorescence signal intensity was observed, due to acidification of the thylakoid lumen *via* water splitting at PSII (Teuber et al. 2001), followed by a gradual fluorescence increase for two minutes until a plateau was reached.This rise in the fluorescence intensity can

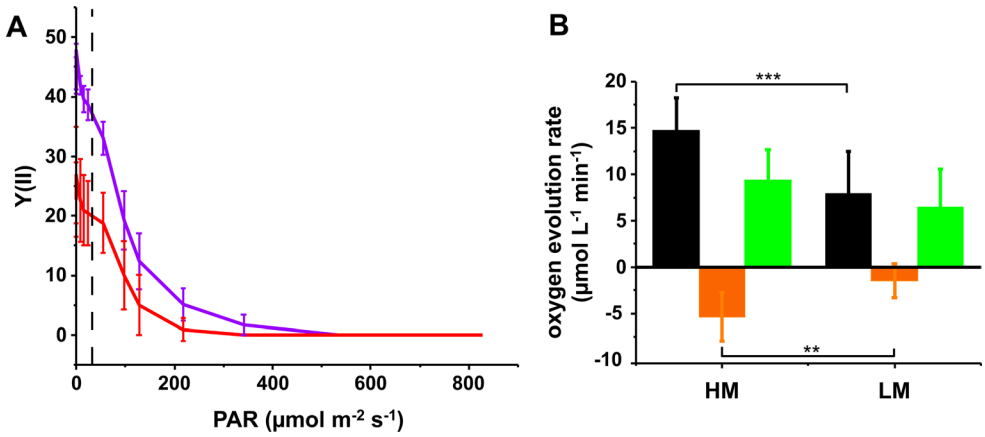

Fig. 6 PSII activity assessed via rapid light curves and oxygen evolution measurements. (**A**) The PSII quantum yields Y(II) were significantly lower when cells were grown under LM (red) compared to HM (blue) conditions The growth light intensity is marked with a dashed line. Error bars represent means ± SD ($N=3$ (HM); $N=5$ (LM)). (**B**) O_2 evolution (green), O_2 consumption (orange), and net O_2 production (black) rates determined analysing HM and LM grown cultures, respectively, under high light at $OD_{750}=2.0$. Error bars represent means ± SD ($N=5$ (HM); $N=7$ (LM)). Significant differences (according to Student's t-test) are indicated as: ** $p<0.01$ and *** $p<0.001$

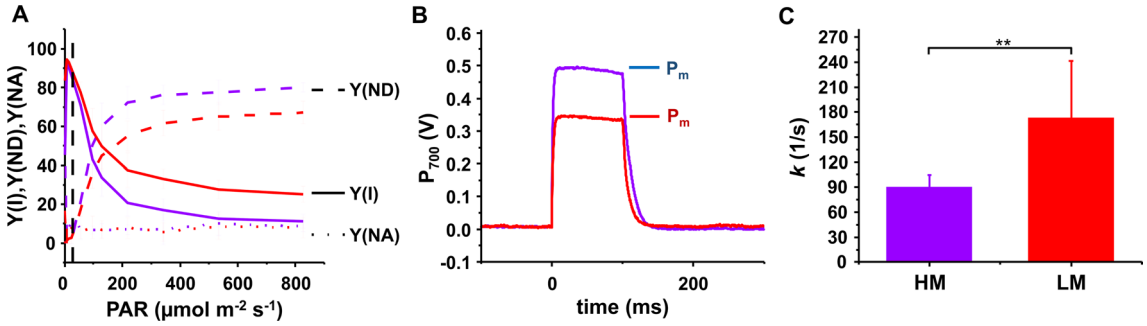

Fig. 7 PSI activity assessed via rapid light curves and P_{700}/ P_{700}^+ oxidation/re-reduction kinetics (**A**) Light intensity dependence of PSI activity: The effective quantum yield Y(I) is affected by donor side limitation Y(ND), which means a lack of electrons to reduce P_{700}^+, and by acceptor side limitation, in which P_{700} cannot be oxidized to P_{700}^+ as the acceptor is reduced. Y(I) (solid line), Y(ND) (dashed line), and Y(NA) (dotted line) in HM (purple) or LM (red) grown *Synechocystis*. The growth light intensity is marked with the dashed black vertical line. Higher Y(I) values were determined under LM conditions due to lowered Y(ND). Error bars represent means ± SD ($N = 3$ (HM); $N = 5$ (LM)). (**B**) P_{700}/P_{700}^+ oxidation/re-reduction kinetic traces of HM (purple) and LM (red) grown *Synechocystis.* Oxidation of P_{700} was induced by a 100 ms saturating pulse with an intensity of 10,000 µmol photons m^{-2} s^{-1}. 10 and 5 independent traces were baseline corrected and averaged from HM and LM grown cultures, respectively. The reduced abundance of PSI in the LM cultures is manifested as a reduced P_m value. (**C**) Traces from (**B**) were fitted with a single exponential decay, and the determined rate constants (k [1/s]) are shown. P_{700}^+ re-reduction was faster when cells were grown under Mg^{2+} limitation consistent with the lower Y(ND). Error bars represent means ± SD. Significant differences (Student's t-test) are indicated as: ** $p < 0.01$

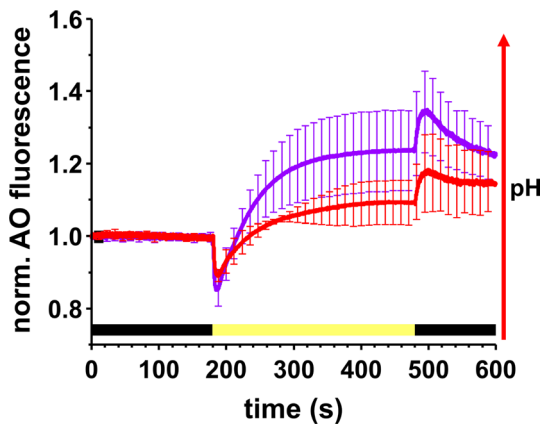

Fig. 8 ΔpH formation across the thylakoid membranes in HM and LM grown *Synechocystis* cells. Changes in the trans-thylakoid pH gradient were monitored *via* AO fluorescence in HM (purple) or LM grown (red) *Synechocystis*. The color bar below the curve indicates the dark (black) - light (yellow) - dark (black) transition. After recording AO fluorescence in the dark for three minutes, cells were exposed to actinic light for five minutes, followed by a two-minute dark period. Error bars represent means ± SD ($N = 15$ (HM); $N = 4$ (LM))

be interpreted as an alkalization of the cytoplasm (Teuber et al. 2001). Upon switching the light off, the fluorescence intensity rapidly increased, indicating re-alkalization of the thylakoid lumen, followed by a slow signal decrease. It should be noted that, because the periplasm was buffered to pH 8.0, the influx of protons from the periplasm into the cytoplasm was limited. Thus, a complete signal recovery cannot be expected. The overall pattern of the AO fluorescence emission changes was similar for HM and LM grown *Synechocystis* cells. However, while acidification of the TM lumen *via* water splitting was only slightly affected, in perfect agreement with the essentially unchanged PSII content per cell, a much lower plateau was reached upon illumination of LM grown cells, suggesting a reduced alkalization of the cytoplasm. Thus, a reduced amount of available Mg^{2+} apparently significantly affects generation of the ΔpH across the TM, albeit PSII acidified the thylakoid lumen to a similar extent at both HM and LM conditions.

Discussion

Mg^{2+} is crucial for growth and development of *Synechocystis* cells. Decreasing Mg^{2+} concentrations in the growth medium led to an increased doubling time (Fig. 2), yet *Synechocystis* cells can still grow at Mg^{2+} concentrations as low as 10 µM. Such ability to adapt to very low Mg^{2+} concentrations was previously noticed for the cyanobacterium *S. elongatus* (Utkilen 1982). While growth was only little affected at Mg^{2+} concentrations of 50 µM and above, cells grown at lower concentrations did not reach saturation levels observed with cells grown at higher Mg^{2+} concentrations. The extended lag phase observed at low Mg^{2+} concentrations suggests that the cellular metabolism adapted to the new growth condition (Bertrand 2019). Since the growth of *Synechocystis* appeared to be only slightly affected in a medium containing 50 µM Mg^{2+}, this concentration was used in all further measurements.

In several non-photosynthetic bacteria (Webb 1951; Brock 1962) and in the cyanobacterium *S. elongatus* (Utkilen 1982), Mg^{2+} limitation impairs cell division. While the Mg^{2+} concentration was high enough in our experiments to not affect cell division, EM images clearly revealed an enlarged EPS layer (Fig. 3). The formation of EPSs in

biofilms typically correlates with the ability to cope with changing environmental conditions (Pereira et al. 2009; De Philippis et al. 2011; Rossi and De Philippis 2015). Former observations suggest a link between Mg^{2+} deficiency and increased EPS formation, as this response was also observed in the cyanobacterium *Cyanospira capsulata* (De Philippis et al. 1991) as well as in *Pseudomonas aeruginosa* (Mulcahy and Lewenza 2011). EPS chelates bivalent cations, (De Philippis et al. 2011) and it has been suggested that *Microcystis flos-aquae* C3-40 accumulates Fe^{2+}/Fe^{3+} and Mn^{2+} in the polysaccharide capsule (Parker et al. 1996). Thus, the increased EPS layer may assist *Synechocystis* in accumulating Mg^{2+} in its immediate environment at LM conditions.

Mg^{2+}limitation causes changes in cell pigmentation, a reduced amount of PSI, and changed energy distribution between the photosystems

As Mg^{2+} is the central ion of Chl molecules, lowering the Mg^{2+} concentration in the growth medium was expected to affect the amount of pigments per cell, as has been observed in plant and algae chloroplasts (Finkle and Appleman 1953; Volgusheva et al. 2015; Kobayashi and Tanoi 2015; Peng et al. 2019; Giraldo et al. 2021), as well as in the cyanobacterium *S. elongatus* (Utkilen 1982). Indeed, in *Synechocystis* cells grown in LM medium the Chl *a* content was significantly reduced (Fig. 4). The concentration and the intracellular transport of Mg^{2+} are tightly regulated, and as free Mg^{2+} is involved in various cellular processes, its cellular level is of special relevance (Maguire 1990). Therefore, it is likely that the overall concentration of Chl *a* decreased in order to mobilize Mg^{2+} and to not lower the total amount of free Mg^{2+} too dramatically, as has been observed in rice (Peng et al. 2019). The decreased cellular Chl *a* content was mainly due to a reduction in PSI abundance (see above). This resulted in the observed decrease in the PSI-to-PSII ratio, as seen in the 77 K fluorescence emission spectra (Fig. 4B). A reduction in the PSI level at LM conditions appears to be reasonable in *Synechocystis*, as most Chl *a* is bound to PSI due to a high PSI-to-PSII ratio (2:1 to 5:1 under standard conditions, (Shen et al. 1993; Murakami 1997), and the observation that each PSI unit contains about 100 Chl *a* molecules (Jordan et al. 2001; Malavath et al. 2018), whereas PSII binds only about 35 (Umena et al. 2011; Gisriel et al. 2022). Analogously, a reduction in the PSI content has also been proposed/observed in plant chloroplasts under Mg^{2+} limitation (Hermans et al. 2004; Farhat et al. 2015). Such a reduction in PSI was previously observed under several stress conditions. A decrease in PSI has long been known as a response when *Synechocystis* cells are shifted from low to high light conditions, presumably to reduce the production of reactive oxygen species (Fujita 1997; Hihara et al. 1998; Sonoike et al. 2001). Furthermore, the PSI abundance is reduced when electron transfer is impaired (Schneider et al. 2001) or cells are grown under iron starvation to prevent oxidative stress (Fraser et al. 2013). Altered PSI-to-PSII ratios are often observed when cells are stressed and in fact the relative enrichment of carotenoids (Fig. 4 and Supplementary Fig. 1BC) further supports cellular stress, as carotenoids play a crucial role in preventing oxidative damage (Steiger et al. 1999; Zakar et al. 2017). In cyanobacteria, carotenoid-binding proteins are heavily involved in preventing overexcitation by regulating the energy transfer from the PBS to the PSs (Kirilovsky et al. 2014). The absorption of blue-green light by the carotenoid bound to the orange carotenoid protein (OCP) induces conformational changes, allowing the protein to bind to the PBS and dissipate excess energy as heat (Wilson et al. 2008; Gwizdala et al. 2011) and the bound carotenoids of the High Light-Inducible Carotenoid-Binding Protein Complex (HLCC) also prevent oxidative damage (Daddy et al. 2015).

Besides a changed Chl *a*-to-Car ratio, we also observed an increase in the PC-to-Chl *a* ratio at LM conditions (Fig. 4A). The decreased PSI content and the increased PC-to-Chl *a* ratio have caused a shift in the energy distribution between the two PSs, as observed via 77 K fluorescence emission spectroscopy (Fig. 4BC). Due to the increased PC-to-Chl *a* ratio and the decreased PSI amount (Fig. 4AB), PBS-to-PSII energy transfer is enhanced. Furthermore, the increased fluorescence emission at 685 nm (relative to the 695 nm) observed in the 77 K fluorescence emsission spectra upon excitation of Chl *a* at 435 nm (Fig. 4C) suggests uncoupled PBS´s, as the PBS terminal emitter also emits light at 685 nm (Mullineaux 1994; Barthel et al. 2013; Kłodawska et al. 2020). PBS uncoupling is commonly caused by environmental stresses, such as heat or high irradiance (Kirilovsky et al. 2014). This process could help preventing over-excitation of the electron transport chain (Tamary et al. 2012), which likely occurs at LM due to the altered PSI-to-PSII ratio.

Changes in PSI-to-PSII stoichiometry alter electron transport properties in LM grown Synechocystis

The increase in the PBS to PSII energy transfer as well as the presence of potentially uncoupled PBS under LM conditions perfecely explain the higher F_o and F_m signals observed in the fluorescence induction curves (Fig. 5B). For instance, high F_o signals were previously observed in *Synechococcus* sp. PCC7942 when the PC-to-Chl ratio was high (Campbell et al. 1996). A reduced F_v/F_m value was also previously observed in plants grown under Mg^{2+} deficiency (Hermans et al. 2004; Yang et al. 2012; Tang et al.

2012; Jamali Jaghdani et al. 2021). Generally, a decreased F_v/F_m ratio is a sign of cellular stress or damage associated with PSII (Maxwell and Johnson 2000; Murchie and Lawson 2013), might indicating a reduced PSII content in LM grown cells.

However, the PSII activity, quantified as O_2 evolution rates, under LM conditions was rather unaffected, while the O_2 consumption rates in LM grown cells were significantly decreased (Fig. 6B). In terms of quantum efficiency, the effective quantum yields of both PSs were influenced by Mg^{2+} limitation, though to different extents. We observed a substantial decrease in the PSII quantum yield, Y(II) (Fig. 6A), in accordance with the decreased F_v/F_m ratios. Such decrease in Y(II) has also been reported for barley chloroplasts (Jamali Jaghdani et al. 2021) and the cyanobacterium *Arthrospira platensis* Gomont 1892 grown at low Mg^{2+} concentrations (Urek and Kerimoglu 2019). As the PSII content per cell appears to be largely unaffected by the LM growth conditions, the decreased F_v/F_m ratio can be explained by an increased basic and steady state fluorescence and/or a more reduced PQ pool upon illumination. Concomitantly, we observed a simultaneous increase in the effective quantum yields of PSI Y(I) under LM conditions (Fig. 7A), mainly due to a decrease in Y(ND), which is consistent with the decrease in the PSI-to-PSII ratio. As recently shown, the P_{700}^+ reduction kinetics mostly slowed down when the amount of PSI was decreased (Moore and Vermaas 2024), and thus the altered ΔpH across TMs might play a role in increasing the P_{700}^+ re-reduction rates. In fact, using an uncoupler results in increased electron transport rates with a simultaneous decrease in ΔpH (Evron and McCarty 2000) which, in turn, results in lower Y(ND) and faster P_{700}^+ re-reduction kinetics. In accordance, we observed a lower light-induced ΔpH across the TM under LM condition (Fig. 8). Therefore, the faster P_{700}^+ re-reduction rates (Fig. 7C) and lower Y(ND) (Fig. 7A) observed under Mg^{2+} limiting conditions are likely due to both an decreased PSI-to-PSII ratio and a lower ΔpH.

Mg^{2+} deficiency results in a decreased transmembrane ΔpH

The above described changes, including lower F_v/F_m and Y(II), along with an increased Y(I), were accompanied by an altered pattern of ΔpH formation across *Synechocystis* membranes (Fig. 8), including a much lower alkalization of the cytoplasm in cells grown under LM conditions compared to HM conditions. When a pH gradient is formed across the TMs upon illumination, the concomitantly generated transmembrane electric potential is balanced by Mg^{2+} and K^+ flux from the lumen to the cytoplasm plus Cl^- flux in the opposite direction (Dilley and Vernon 1965; Hind et al. 1974; Chow et al. 1976; Lyu and Lazár 2017). Therefore, when cells were grown under LM conditions, altered Mg^{2+} concentrations in the cytoplasm and/or lumen may impair proton flux across the TM. Based on AO measurements performed with a *Synechocystis* mutant where a predominantly TM-localized potassium channel (*Syn*K) was deleted, the acidification of the lumen was less pronounced upon illumination compared to the wild type (Checchetto et al. 2012). Likewise, the reduced ΔpH observed in LM cells could well be caused by the reduced Mg^{2+} concentration, and thus, reduced Mg^{2+} flux across the TM.

According to the AO measurements, the signal increase, reflecting alkalization of the cytoplasm, was only about half in size in LM grown cells compared with cells grown under HM conditions. The light-induced alkalization of the cytoplasm is achieved by proton pumping to the TM lumen by electron transport-coupled proton translocation and also by proton extrusion through the CM (Teuber et al. 2001). Proton extrusion across the CM is the result of respiration as well as ATP hydrolysis (Teuber et al. 2001) and/or proton extrusion by the PxcA (former CotA) protein driven by a still unknown mechanism (Katoh et al. 1996; Sonoda et al. 1998; Inago et al. 2020). Therefore, the impaired respiration observed in cells grown under LM conditions (Fig. 6B) may also contribute to the alterations in the AO fluorescence signal, finally affecting the PSI activity (see above).

Upon switching the light off, a fast increase in the AO fluorescence intensity was observed, which is most likely due to a rapid re-alkalization of the lumen. According to Teuber et al. (Teuber et al. 2001), the subsequent signal decrease in the dark may reflect the consumption of redox equivalents. Since many enzymes in the Calvin–Benson–Bassham cycle require Mg^{2+} as a cofactor and alkalization of the lumen for proper function (Lorimer et al. 1976; Flügge et al. 1980; Mott and Berry 1986), a lowered cellular concentration of Mg^{2+} could be a cause for the less pronounced AO signal decrease.

Conclusion

Mg^{2+} is the central ion of Chl molecules, and thus a significant amount of the intracellular Mg^{2+} is part of Chl molecules in cyanobacteria. Accordingly, the Chl *a* content per cell was significantly lowered when *Synechocystis* cells were grown in LM medium. This reduction in Chl led to a remarkably decreased PSI content, and related changes in electron transport properties. Additionally, Mg^{2+} limitation resulted in an altered pH gradient build up across the TM under illumination.

Supplementary Information The online version contains supplementary material available at https://doi.org/10.1007/s11120-

024-01112-7.

Acknowledgements We thank Renate Genswein, Annette Roth, Fine Flecks, and Rita Grotjahn for technical assistance.

Author contributions D.S. and A-C.P. designed experiments. D.S., A-C.P., G.B., and S.G. performed experiments, analyzed data, and discussed results. D.S.: Funding Acquisition, Project Administration, Resources, Supervision. A-C.P. and D.S. drafted the manuscript and all authors edited, reviewed and approved the final version of the manuscript.

Funding Open Access funding enabled and organized by Projekt DEAL.

Data availability No datasets were generated or analysed during the current study.

Declarations

Competing interests The authors declare no competing interests.

Open Access This article is licensed under a Creative Commons Attribution 4.0 International License, which permits use, sharing, adaptation, distribution and reproduction in any medium or format, as long as you give appropriate credit to the original author(s) and the source, provide a link to the Creative Commons licence, and indicate if changes were made. The images or other third party material in this article are included in the article's Creative Commons licence, unless indicated otherwise in a credit line to the material. If material is not included in the article's Creative Commons licence and your intended use is not permitted by statutory regulation or exceeds the permitted use, you will need to obtain permission directly from the copyright holder. To view a copy of this licence, visit http://creativecommons.org/licenses/by/4.0/.

References

Andrizhiyevskaya EG, Chojnicka A, Bautista JA et al (2005) Origin of the F685 and F695 fluorescence in Photosystem II. Photosynth Res 84:173–180. https://doi.org/10.1007/s11120-005-0478-7

Barber J, Mills J, Nicolson J (1974) Studies with cation specific ionophores show that within the intact chloroplast mg++acts as the main exchange cation for H+pumping. FEBS Lett 49:106–110. https://doi.org/10.1016/0014-5793(74)80643-5

Barthel S, Bernát G, Seidel T et al (2013) Thylakoid membrane maturation and PSII activation are linked in Greening Synechocystis sp. PCC 6803 cells. Plant Physiol 163:1037–1046. https://doi.org/10.1104/pp.113.224428

Belkin S, Mehlhorn RJ, Packer L (1987) Proton gradients in intact cyanobacteria. Plant Physiol 84:25–30. https://doi.org/10.1104/pp.84.1.25

Bertrand RL (2019) Lag phase is a dynamic, organized, adaptive, and evolvable period that prepares bacteria for cell division. J Bacteriol 201:1–21. https://doi.org/10.1128/JB.00697-18

Brock TD (1962) Effects of magnesium ion deficiency on Escherichia coli and possible relation to the mode of action of novobiocin. J Bacteriol 84:679–682. https://doi.org/10.1128/jb.84.4.679-682.1962

Cakmak I, Kirkby EA (2008) Role of magnesium in carbon partitioning and alleviating photooxidative damage. Physiol Plant 133:692–704. https://doi.org/10.1111/j.1399-3054.2007.01042.x

Calzadilla PI, Kirilovsky D (2020) Revisiting cyanobacterial state transitions. Photochem Photobiol Sci 19:585–603. https://doi.org/10.1039/c9pp00451c

Campbell D, Bruce D, Carpenter C et al (1996) Two forms of the photosystem II D1 protein alter energy dissipation and state transitions in the cyanobacterium Synechococcus sp. PCC 7942. Photosynth Res 47:131–144. https://doi.org/10.1007/BF00016176

Campbell D, Hurry V, Clarke AK et al (1998) Chlorophyll fluorescence analysis of Cyanobacterial Photosynthesis and Acclimation. Microbiol Mol Biol Rev 62:667–683. https://doi.org/10.1128/mmbr.62.3.667-683.1998

Checchetto V, Segalla A, Allorent G et al (2012) Thylakoid potassium channel is required for efficient photosynthesis in cyanobacteria. Proc Natl Acad Sci 109:11043–11048. https://doi.org/10.1073/pnas.1205960109

Chow W, Wagner A, Hope A (1976) Light-dependent redistribution of ions in isolated spinach chloroplasts. Australian J Plant Physiol 3:853–861. https://doi.org/10.1071/PP9760853

Daddy S, Zhan J, Jantaro S et al (2015) A novel high light-inducible carotenoid-binding protein complex in the thylakoid membranes of Synechocystis PCC 6803. Sci Rep 5:9480. https://doi.org/10.1038/srep09480

De Philippis R, Sili C, Tassinato G et al (1991) Effects of growth conditions on exopolysaccharide production by Cyanospira capsulata. Bioresour Technol 38:101–104. https://doi.org/10.1016/0960-8524(91)90138-A

De Philippis R, Margheri MC, Pelosi E, Ventura S (1993) Exopolysaccharide production by a unicellular cyanobacterium isolated from a hypersaline habitat. J Appl Phycol 5:387–394. https://doi.org/10.1007/BF02182731

De Philippis R, Colica G, Micheletti E (2011) Exopolysaccharide-producing cyanobacteria in heavy metal removal from water: molecular basis and practical applicability of the biosorption process. Appl Microbiol Biotechnol 92:697–708. https://doi.org/10.1007/s00253-011-3601-z

Dilley RA, Vernon LP (1965) Ion and water transport processes related to the light-dependent shrinkage of spinach chloroplasts. Arch Biochem Biophys 111:365–375. https://doi.org/10.1016/0003-9861(65)90198-0

Evron Y, McCarty RE (2000) Simultaneous measurement of ΔpH and electron transport in chloroplast thylakoids by 9-aminoacridine fluorescence. Plant Physiol 124:407–414. https://doi.org/10.1104/pp.124.1.407

Farhat N, Ivanov AG, Krol M et al (2015) Preferential damaging effects of limited magnesium bioavailability on photosystem I in Sulla carnosa plants. Planta 241:1189–1206. https://doi.org/10.1007/s00425-015-2248-x

Finkle BJ, Appleman D (1953) The Effect of Magnesium Concentration on Chlorophyll and Catalase Development in Chlorella. Plant Physiol 28:652–663. https://doi.org/10.1104/pp.28.4.652

Flatman PW (1984) Magnesium transport across cell membranes. J Membr Biol 80:1–14. https://doi.org/10.1007/BF01868686

Flügge UI, Freisl M, Heldt HW (1980) The mechanism of the control of carbon fixation by the pH in the chloroplast stroma: studies with acid mediated proton transfer across the envelope. Planta 149:48–51. https://doi.org/10.1007/BF00386226

Fraser JM, Tulk SE, Jeans JA et al (2013) Photophysiological and photosynthetic complex changes during Iron starvation in Synechocystis sp. PCC 6803 and Synechococcus elongatus PCC 7942. PLoS ONE 8:e59861. https://doi.org/10.1371/journal.pone.0059861

Fujita Y (1997) A study on the dynamic features of photosystem stoichiometry: accomplishments and problems for future studies. Photosynthesis Research 53, 83–93.

Genty B, Briantais J-M, Baker NR (1989) The relationship between the quantum yield of photosynthetic electron transport and

quenching of chlorophyll fluorescence. Biochimica et Biophysica Acta (BBA). - Gen Subj 990:87–92. https://doi.org/10.1016/S0304-4165(89)80016-9

Giraldo ND, Correa SM, Arbeláez A et al (2021) Reducing self-shading effects in Botryococcus braunii cultures: effect of Mg2 + deficiency on optical and biochemical properties, photosynthesis and lipidomic profile. Bioresources Bioprocess 8:33. https://doi.org/10.1186/s40643-021-00389-z

Gisriel CJ, Wang J, Liu J et al (2022) High-resolution cryo-electron microscopy structure of photosystem II from the mesophilic cyanobacterium, Synechocystis sp. PCC 6803. Proc Natl Acad Sci 119. https://doi.org/10.1073/pnas.2116765118

Gray MW (1989) The evolutionary origins of organelles. Trends Genet 5:294–299. https://doi.org/10.1016/0168-9525(89)90111-X

Gwizdala M, Wilson A, Kirilovsky D (2011) In Vitro reconstitution of the Cyanobacterial Photoprotective mechanism mediated by the Orange Carotenoid Protein in Synechocystis PCC 6803. Plant Cell 23:2631–2643. https://doi.org/10.1105/tpc.111.086884

Hall JD, Barr R, Al-Abbas AH, Crane FL (1972) The ultrastructure of chloroplasts in Mineral-deficient Maize leaves. Plant Physiol 50:404–409. https://doi.org/10.1104/pp.50.3.404

Hermans C, Johnson GN, Strasser RJ, Verbruggen N (2004) Physiological characterisation of magnesium deficiency in sugar beet: acclimation to low magnesium differentially affects photosystems I and II. Planta 220:344–355. https://doi.org/10.1007/s00425-004-1340-4

Hihara Y, Sonoike K, Ikeuchi M (1998) A novel gene, pmgA, specifically regulates photosystem stoichiometry in the cyanobacterium Synechocystis species PCC 6803 in response to high light. Plant Physiol 117:1205–1216. https://doi.org/10.1104/pp.117.4.1205

Hind G, Nakatani HY, Izawa S (1974) Light-Dependent Redistribution of Ions in Suspensions of Chloroplast Thylakoid Membranes. Proceedings of the National Academy of Sciences 71:1484–1488. https://doi.org/10.1073/pnas.71.4.1484

Inago H, Sato R, Masuda S (2020) Regulation of light-induced H + extrusion and uptake by cyanobacterial homologs of the plastidial FLAP1, DLDG1, and Ycf10 in Synechocystis sp. PCC6803. Biochimica et Biophysica Acta (BBA) -. Bioenergetics 1861:148258. https://doi.org/10.1016/j.bbabio.2020.148258

Jamali Jaghdani S, Jahns P, Tränkner M (2021) Mg deficiency induces photo-oxidative stress primarily by limiting CO2 assimilation and not by limiting photosynthetic light utilization. Plant Sci 302. 110751. https://doi.org/10.1016/j.plantsci.2020.110751

Jennings RC, Forti G, Gerola PD, Garlaschi FM (1978) Studies on cation-induced Thylakoid membrane stacking, fluorescence yield, and Photochemical Efficiency. Plant Physiol 62:879–884. https://doi.org/10.1104/pp.62.6.879

Jordan P, Fromme P, Witt HT et al (2001) Three-dimensional structure of cyanobacterial photosystem I at 2.5 Å resolution. Nature 411:909–917. https://doi.org/10.1038/35082000

Kaňa R, Govindjee (2016) Role of ions in the regulation of light-harvesting. Front Plant Sci 7:1849. https://doi.org/10.3389/fpls.2016.01849

Katoh A, Sonoda M, Katoh H, Ogawa T (1996) Absence of light-induced proton extrusion in a cota-less mutant of Synechocystis sp. Strain PCC6803. J Bacteriol 178:5452–5455. https://doi.org/10.1128/jb.178.18.5452-5455.1996

Kirilovsky D, Kaňa R, Prášil O (2014) Mechanisms Modulating Energy Arriving at Reaction Centers in Cyanobacteria. In: Demmig-Adams B, Garab G, Adams IIIW, Govindjee (eds) Non-photochemical quenching and energy dissipation in plants, Algae and Cyanobacteria. Springer Netherlands, Dordrecht, pp 471–501

Kitajima M, Butler WL (1975) Quenching of chlorophyll fluorescence and primary photochemistry in chloroplasts by dibromothymoquinone. Biochimica et Biophysica Acta (BBA) -. Bioenergetics 376:105–115. https://doi.org/10.1016/0005-2728(75)90209-1

Kłodawska K, Kovács L, Vladkova R et al (2020) Trimeric organization of photosystem I is required to maintain the balanced photosynthetic electron flow in cyanobacterium Synechocystis sp. PCC 6803. Photosynth Res 143:251–262. https://doi.org/10.1007/s11120-019-00696-9

Klughammer C, Schreiber U (1994) An improved method, using saturating light pulses, for the determination of photosystem I quantum yield via P700+-absorbance changes at 830 nm. Planta 192:261–268. https://doi.org/10.1007/BF00194461

Klughammer C, Schreiber U (2008) Saturation pulse method for assessment of energy conversion in PS I. PAM Application Notes 1:11–14

Kobayashi NI, Tanoi K (2015) Critical issues in the study of magnesium transport systems and magnesium deficiency symptoms in plants. Int J Mol Sci 16:23076–23093. https://doi.org/10.3390/ijms160923076

Kung FC, Raymond J, Glaser DA (1976) Metal ion content of Escherichia coli versus cell age. J Bacteriol 126:1089–1095. https://doi.org/10.1128/jb.126.3.1089-1095.1976

Liu LN (2016) Distribution and dynamics of electron transport complexes in cyanobacterial thylakoid membranes. Biochim et Biophys Acta - Bioenergetics 1857:256–265. https://doi.org/10.1016/j.bbabio.2015.11.010

Lorimer GH, Badger MR, Andrews TJ (1976) The activation of Ribulose-1,5-bisphosphate carboxylase by Carbon Dioxide and Magnesium Ions. Equilibria, Kinetics, a suggested mechanism, and physiological implications. Biochemistry 15:529–536. https://doi.org/10.1021/bi00648a012

Luimstra VM, Schuurmans JM, de Carvalho CFM et al (2019) Exploring the low photosynthetic efficiency of cyanobacteria in blue light using a mutant lacking phycobilisomes. Photosynth Res 141:291–301. https://doi.org/10.1007/s11120-019-00630-z

Lusk JE, Williams RJP, Kennedy EP (1968) Magnesium and the growth of Escherichia coli. J Biol Chem 243:2618–2624

Lyu H, Lazár D (2017) Modeling the light-induced electric potential difference ΔΨ across the thylakoid membrane based on the transition state rate theory. Biochim et Biophys Acta (BBA) - Bioenergetics 1858:239–248. https://doi.org/10.1016/j.bbabio.2016.12.009

Maguire ME (1990) Magnesium: A Regulated and Regulatory Cation. In: Sigel H, Sigel A (eds) Metal ions in biological systems, 26th edn. Dekker, pp 135–153

Maguire ME, Cowan JA (2002) Magnesium chemistry and biochemistry. Biometals 15:203–210. https://doi.org/10.1023/a:1016058229972

Malavath T, Caspy I, Netzer-El SY et al (2018) Structure and function of wild-type and subunit-depleted photosystem I in *Synechocystis*. Biochim et Biophys Acta - Bioenergetics 1859:645–654. https://doi.org/10.1016/j.bbabio.2018.02.002

Maxwell K, Johnson GN (2000) Chlorophyll fluorescence—a practical guide. J Exp Bot 51:659–668. https://doi.org/10.1093/jxb/51.345.659

Mereschkowsky C (1905) Über Natur und Ursprung Der Chromatophoren Im Pflanzenreiche. Biologisches Centralblatt 25:593–604

Merhaut DJ (2007) Magnesium. In: Barker AV, Pilbeam DJ (eds) Handbook of Plant Nutrition. CRC, Boca Raton, pp 145–181

Mitchell P (1961) Coupling of phosphorylation to Electron and Hydrogen Transfer by a Chemi-osmotic type of mechanism. Nature 191:144–148. https://doi.org/10.1038/191144a0

Moncany MLJ, Kellenberger E (1981) High magnesium content of Escherichia coli B. Experientia 37:846–847. https://doi.org/10.1007/BF01985672

Moore V, Vermaas W (2024) Functional consequences of modification of the photosystemI/photosystem II ratio in the cyanobacterium Synechocystis sp.PCC 6803. J Bacteriol 206:e0045423. https://doi.org/10.1128/jb.00454-23

Mott KA, Berry JA (1986) Effects of pH on activity and activation of Ribulose 1,5-Bisphosphate carboxylase at Air Level CO 2. Plant Physiol 82:77–82. https://doi.org/10.1104/pp.82.1.77

Mulcahy H, Lewenza S (2011) Magnesium limitation is an environmental trigger of the Pseudomonas aeruginosa biofilm lifestyle. PLoS ONE 6:e23307. https://doi.org/10.1371/journal.pone.0023307

Mullineaux CW (1994) Excitation energy transfer from phycobilisomes to Photosystem I in a cyanobacterial mutant lacking Photosystem II. BBA - Bioenergetics 1184:71–77. https://doi.org/10.1016/0005-2728(94)90155-4

Mullineaux CW (2014) Co-existence of photosynthetic and respiratory activities in cyanobacterial thylakoid membranes. Biochim et Biophys Acta - Bioenergetics 1837:503–511. https://doi.org/10.1016/j.bbabio.2013.11.017

Mullineaux CW, Allen JF (1990) State 1-State 2 transitions in the cyanobacterium Synechococcus 6301 are controlled by the redox state of electron carriers between Photosystems I and II. Photosynth Res 23:297–311. https://doi.org/10.1007/BF00034860

Murakami A (1997) Quantitative analysis of 77K fluorescence emission spectra in Synechocystis sp. PCC 6714 and Chlamydomonas reinhardtii with variable PS I/PS II stoichiometries. Photosynth Res 53:141–148. https://doi.org/10.1023/A:1005818317797

Murchie EH, Lawson T (2013) Chlorophyll fluorescence analysis: a guide to good practice and understanding some new applications. J Exp Bot 64:3983–3998. https://doi.org/10.1093/jxb/ert208

Parker DL, Schram BR, Plude JL, Moore RE (1996) Effect of metal cations on the viscosity of a pectin-like capsular polysaccharide from the cyanobacterium Microcystis Flos-Aquae C3-40. Appl Environ Microbiol 62:1208–1213. https://doi.org/10.1128/aem.62.4.1208-1213.1996

Peng YY, Liao LL, Liu S et al (2019) Magnesium deficiency triggers sgr-mediated chlorophyll degradation for magnesium remobilization. Plant Physiol 181:262–275. https://doi.org/10.1104/pp.19.00610

Pereira S, Zille A, Micheletti E et al (2009) Complexity of cyanobacterial exopolysaccharides: composition, structures, inducing factors and putative genes involved in their biosynthesis and assembly. FEMS Microbiol Rev 33:917–941. https://doi.org/10.1111/j.1574-6976.2009.00183.x

Peschek GA, Czerny T, Schmetterer G, Nitschmann WH (1985) Transmembrane Proton Electrochemical Gradients in Dark Aerobic and anaerobic cells of the cyanobacterium (Blue-Green Alga) Anacystis nidulans: evidence for Respiratory Energy Transduction in the plasma membrane. Plant Physiol 79:278–284. https://doi.org/10.1104/pp.79.1.278

Pohland A-C, Schneider D (2019) Mg2 + homeostasis and transport in cyanobacteria – at the crossroads of bacterial and chloroplast Mg2 + import. Biol Chem 400:1289–1301. https://doi.org/10.1515/hsz-2018-0476

Porra RJ, Thompson WA, Kriedemann PE (1989) Determination of accurate extinction coefficients and simultaneous equations for assaying chlorophylls a and b extracted with four different solvents: verification of the concentration of chlorophyll standards by atomic absorption spectroscopy. Biochim et Biophys Acta (BBA) - Bioenergetics 975:384–394. https://doi.org/10.1016/S0005-2728(89)80347-0

Portis ARJ (1992) Regulation of ribulose 1,5-bisphosphate carboxylase/oxygenase activity. Annu Rev Plant Physiol Plant Mol Biol 43:415–437. https://doi.org/10.1146/annurev.pp.43.060192.002215

Portis ARJ, Heldt HW (1976) Light-dependent changes of the Mg2 + concentration in the stroma in relation to the Mg2 + dependency of CO2 fixation in intact chloroplasts. Biochim et Biophys Acta (BBA) - Bioenergetics 449:434–446. https://doi.org/10.1016/0005-2728(76)90154-7

Portis ARJ, Chon CJ, Mosbach A, Heldt HW (1977) Fructose-and sedoheptulosebisphosphatase. The sites of a possible control of CO2 fixation by light-dependent changes of the stromal Mg2 + concentration. Biochimica et Biophysica Acta (BBA) -. Bioenergetics 461:313–325. https://doi.org/10.1016/0005-2728(77)90181-5

Pottosin I, Dobrovinskaya O (2015) Ion channels in native Chloroplast membranes: challenges and potential for Direct Patch-Clamp studies. Front Physiol 6:396. https://doi.org/10.3389/fphys.2015.00396

Rakhimberdieva MG, Boichenko VA, Karapetyan NV, Stadnichuk IN (2001) Interaction of phycobilisomes with photosystem II dimers and photosystem I monomers and trimers in the cyanobacterium Spirulina platensis. Biochemistry 40:15780–15788. https://doi.org/10.1021/bi010009t

Reynolds ES (1963) The use of lead citrate at high pH as an electron-opaque stain in electron microscopy. J Cell Biol 17:208–212. https://doi.org/10.1083/jcb.17.1.208

Rijgersberg CP, Amesz J (1980) Fluorescence and energy transfer in phycobiliprotein-containing algae at low temperature. Biochimica et Biophysica Acta (BBA) -. Bioenergetics 593:261–271. https://doi.org/10.1016/0005-2728(80)90064-X

Rippka R, Deruelles J, Waterbury JB et al (1979) Generic assignments, strain histories and properties of pure cultures of Cyanobacteria. Microbiology 111:1–61. https://doi.org/10.1099/00221287-111-1-1

Romani AMP, Scarpa A (2000) Regulation of cellular magnesium. Front Biosci 5:d720. https://doi.org/10.2741/Romani

Rossi F, De Philippis R (2015) Role of Cyanobacterial exopolysaccharides in Phototrophic biofilms and in Complex Microbial mats. Life 5:1218–1238. https://doi.org/10.3390/life5021218

Sagan L (1967) On the origin of mitosing cells. J Theor Biol 14:225–274. https://doi.org/10.1016/0022-5193(67)90079-3

Sakurai I, Shen J-R, Leng J et al (2006) Lipids in Oxygen-Evolving Photosystem II complexes of Cyanobacteria and higher plants. J Biochem 140:201–209. https://doi.org/10.1093/jb/mvj141

Schimper AFW (1883) Ueber die Entwicklung Der Chlorophyllkorner Und Farbkorper. Bot Ztg 41:105–112

Schneider D, Berry S, Rich P et al (2001) A Regulatory Role of the PetM subunit in a Cyanobacterial Cytochrome b6 f complex. J Biol Chem 276:16780–16785. https://doi.org/10.1074/jbc.M009503200

Schreiber U (2004) Pulse-amplitude-modulation (PAM) Fluorometry and Saturation Pulse Method: an overview. In: Papageorgiou GC, Govindjee (eds) Chlorophyll a fluorescence, 19th edn. Springer Netherlands, Dordrecht, pp 279–319

Schreiber U, Endo T, Mi H, Asada K (1995) Quenching analysis of chlorophyll fluorescence by the saturation pulse method: Particular aspects relating to the study of eukaryotic algae and cyanobacteria. Plant Cell Physiol 36:873–882. https://doi.org/10.1093/oxfordjournals.pcp.a078833

Shen G, Boussiba S, Vermaas WFJ (1993) Synechocystis Sp PCC 6803 strains lacking photosystem I and phycobilisome function. Plant Cell 5:1853–1863. https://doi.org/10.2307/3869700

Silver S (1969) Active transport of magnesium in Escherichia coli. Proc Natl Acad Sci 62:764–771. https://doi.org/10.1073/pnas.62.3.764

Sonoda M, Katoh H, Vermaas W et al (1998) Photosynthetic electron transport involved in PxcA-dependent proton extrusion in Synechocystis sp. strain PCC6803: effect of pxcA inactivation on CO2, HCO3-, and NO3- uptake. J Bacteriol 180:3799–3803. https://doi.org/10.1128/jb.180.15.3799-3803.1998

Sonoike K, Hihara Y, Ikeuchi M (2001) Physiological significance of the regulation of Photosystem Stoichiometry upon High Light Acclimation of Synechocystis sp. PCC 6803. Plant Cell Physiol 42:379–384. https://doi.org/10.1093/pcp/pce046

Steiger S, Schäfer L, Sandmann G (1999) High-light-dependent upregulation of carotenoids and their antioxidative properties in the

cyanobacterium Synechocystis PCC 6803. J Photochem Photobiol B 52:14–18. https://doi.org/10.1016/S1011-1344(99)00094-9

Tang N, Li Y, Chen L (2012) Magnesium deficiency–induced impairment of photosynthesis in leaves of fruiting Citrus reticulata trees accompanied by up-regulation of antioxidant metabolism to avoid photo-oxidative damage. J Plant Nutr Soil Sci 175:784–793. https://doi.org/10.1002/jpln.201100329

Teuber M, Rögner M, Berry S (2001) Fluorescent probes for non-invasive bioenergetic studies of whole cyanobacterial cells. Biochim et Biophys Acta (BBA) - Bioenergetics 1506:31–46. https://doi.org/10.1016/S0005-2728(01)00178-5

Tränkner M, Jamali Jaghdani S (2019) Minimum magnesium concentrations for photosynthetic efficiency in wheat and sunflower seedlings. Plant Physiol Biochem 144:234–243. https://doi.org/10.1016/j.plaphy.2019.09.040

Umena Y, Kawakami K, Shen J-R, Kamiya N (2011) Crystal structure of oxygen-evolving photosystem II at a resolution of 1.9 Å. Nature 473:55–60. https://doi.org/10.1038/nature09913

Urek RO, Kerimoglu Y (2019) Evaluation of effects of Mg2 + and Cu2 + on pigment-metabolite production and photosystem II activity of Arthrospira platensis Gomont 1892. Turkish J Fisheries Aquat Sci 19:873–883. https://doi.org/10.4194/1303-2712-v19_10_07

Utkilen HC (1982) Magnesium-limited growth of the Cyanobacterium Anacystis nidulans. Microbiology 128:1849–1862. https://doi.org/10.1099/00221287-128-8-1849

Volgusheva A, Kukarskikh G, Krendeleva T et al (2015) Hydrogen photoproduction in green algae Chlamydomonas reinhardtii under magnesium deprivation. RSC Adv 5:5633–5637. https://doi.org/10.1039/C4RA12710B

Wacker WEC (1969) The biochemistry of magnesium. Ann N Y Acad Sci 162:717–726. https://doi.org/10.1111/j.1749-6632.1969.tb13003.x

Webb M (1951) The influence of Magnesium on Cell Division: 4. The specificity of Magnesium. J Gen Microbiol 5:480–484. https://doi.org/10.1099/00221287-5-3-480

Willstätter R (1906) Zur Kenntniss Der Zusammensetzung Des Chlorophylls. Justus Liebigs Annalen Der Chemie 350:48–82. https://doi.org/10.1002/jlac.19063500103

Wilson A, Punginelli C, Gall A et al (2008) A photoactive carotenoid protein acting as light intensity sensor. Proc Natl Acad Sci 105:12075–12080. https://doi.org/10.1073/pnas.0804636105

Wojdyr M (2010) Fityk: a general-purpose peak fitting program. J Appl Crystallogr 43:1126–1128. https://doi.org/10.1107/S0021889810030499

Yang G-H, Yang L-T, Jiang H-X et al (2012) Physiological impacts of magnesium-deficiency in Citrus seedlings: photosynthesis, antioxidant system and carbohydrates. Trees 26:1237–1250. https://doi.org/10.1007/s00468-012-0699-2

Zakar T, Herman E, Vajravel S et al (2017) Lipid and carotenoid cooperation-driven adaptation to light and temperature stress in Synechocystis sp. PCC6803. Biochim et Biophys Acta - Bioenergetics 1858:337–350. https://doi.org/10.1016/j.bbabio.2017.02.002

Zakar T, Kovacs L, Vajravel S et al (2018) Determination of PS I oligomerisation in various cyanobacterial strains and mutants by non-invasive methods. Photosynthetica 56:294–299. https://doi.org/10.1007/s11099-018-0795-7

Zavrel T, Sinetova M, Červený J (2015) Measurement of Chlorophyll a and carotenoids Concentration in Cyanobacteria. BIO-PROTOCOL 5:1–5. https://doi.org/10.21769/BioProtoc.1467

Publisher's Note Springer Nature remains neutral with regard to jurisdictional claims in published maps and institutional affiliations.